


## Article

# Innovative Adaptive Multiscale 3D Simulation Platform for the Yellow River Using Sphere Geodesic Octree Grid Techniques

Bingxuan Li , Jinxin Wang \*, Yan Zhang and Yongkang Sun

School of Geoscience & Technology, Zhengzhou University, Zhengzhou 450001, China; alinww@126.com (B.L.); zy15565509353@gs.zzu.edu.cn (Y.Z.); sunkyx@163.com (Y.S.)

\* Correspondence: jxwang@zzu.edu.cn

**Abstract:** Earth system simulation technology is fundamental for ecological protection and high-quality development in the Yellow River Basin. To address the lack of a Yellow River simulation platform, this study proposes an adaptive multiscale true 3D crust simulation platform using the Sphere Geodesic Octree Grid (SGOG). Twelve models in four categories were designed: single fine-scale models, geomorphic zone-based models, and models using both top-down and bottom-up approaches. The models were evaluated based on terrain feature representation and computational efficiency. The results show that single fine-scale models preserve detailed terrain features but are computationally intensive. They are suitable for the precise simulation of surface processes. Top-down and bottom-up models balance terrain detail and efficiency, and are thereby widely applicable. Geomorphic zone-based models provide detailed focal area representation and higher computational efficiency, being more targeted. Various methods offer flexible scale transformations, each with its own strengths, allowing researchers to select a method according to practical application needs. Consequently, this research demonstrates that spherical discrete grids offer reliable support for constructing basin simulation platforms, providing new technological and scientific insights for the Yellow River Basin's ecological protection and development.

**Keywords:** global discrete grid; Sphere Geodesic Octree Grid; true 3D geographic scene; adaptive multiscale; Yellow River Basin



**Citation:** Li, B.; Wang, J.; Zhang, Y.; Sun, Y. Innovative Adaptive Multiscale 3D Simulation Platform for the Yellow River Using Sphere Geodesic Octree Grid Techniques. *Water* **2024**, *16*, 1791. <https://doi.org/10.3390/w16131791>

Academic Editor: Pankaj Kumar

Received: 13 May 2024

Revised: 18 June 2024

Accepted: 20 June 2024

Published: 25 June 2024



**Copyright:** © 2024 by the authors. Licensee MDPI, Basel, Switzerland. This article is an open access article distributed under the terms and conditions of the Creative Commons Attribution (CC BY) license (<https://creativecommons.org/licenses/by/4.0/>).

## 1. Introduction

The Yellow River, known as the mother river of the Chinese nation, represents the history of Chinese development [1]. The evolution of the ideas and wisdom of flood control and river management in China can be traced back to evasion, embankment filling, dredging, diversion, embankment reinforcement, coordination, harmony, and protection and development [1]. With the advancement of flood control technologies, from manual labor, animal power, machinery, and electricity to computers, concepts such as the real Yellow River, model Yellow River, digital Yellow River [2], and Yellow River simulators [3] have emerged. Flood control technologies have propelled and guided the scientific and technological development in China. Thus, the philosophy of flood control profoundly influences national governance. Water control is akin to state governance, and the advanced water management civilization of the Chinese nation to a certain extent determines the path to the country's prosperity, comprehensive national strength, and global standing [4].

The watershed simulator represents a new conceptual framework and a significant undertaking in digital water management in the context of contemporary spatial big data and information technology. The Yellow River simulator, designed specifically for the Yellow River Basin, focuses on the Yellow River Basin and serves as an integrated watershed simulation system, with scientific apparatus developed and deployed throughout the basin. It revolves around the natural and social water cycles within the basin, with a focus on addressing key issues related to the Yellow River by coupling multiple systems, coordinating

multiple actors/parties, achieving multiple functionalities, simulating multiple processes, and ensuring integration [3]. The Yellow River simulator enables a comprehensive process simulation of various natural and human factors within the basin, as well as their coupled interactions. It particularly focuses on addressing distinctive Yellow River issues, such as soil erosion, sediment deposition, ecological vulnerability, limited development quality, and social governance capacity [3]. Simulating watershed-scale geographical processes represents the core task of the simulator, with the coupling of temporal and spatial scales being a key and challenging scientific problem [5]. From a conceptual standpoint, watershed simulation can be divided into comprehensive simulation (simulating the response of a watershed system to geographic variable changes) and scenario analysis (analyzing and evaluating the economic and ecological effects of various element combinations, thereby facilitating decision-making in management) [6]. Both the simulations and analyses require a simulation platform as a foundation. In summary, the simulation platform serves as the catalyst, key, and core of the watershed simulator, and all the work of the simulator revolves around the simulation platform.

Watershed simulation belongs to the domain of Earth system simulation, which is an application of Earth simulation at the watershed scale [5]. The Earth's system encompasses various spheres, including the near-Earth space, atmosphere, oceans, land surface, biosphere, and solid Earth (including the lithosphere, mantle, and core). Mathematical equations have been established based on the physical, chemical, and biological processes within these spheres, and large-scale comprehensive computational programs, known as Earth system models, have been developed to solve these equations using numerical methods [7]. Earth system models are among the most complex and comprehensive scientific numerical simulation tools. Their advancement reflects a country's core competitiveness in Earth systems' science research, and serves as an important indicator for assessing the country's overall level of Earth science research and comprehensive national strength [8]. Internationally, the United States, United Kingdom, Germany, Japan, and France hold leading positions in Earth system model development and simulation research. Examples include the Community Earth System Model (CESM) in the United States (National Center for Atmospheric Research, Boulder, CO, USA), the European Network for Earth System Modeling (ENES) (EUDAT Ltd, Keilaranta, Finland), and the Frontiers Research System for Global Change (FRSGC) in Japan (Japan Agency for Marine-Earth Science and Technology (JAMSTEC), Yokohama, Japan) [7]. China's Earth System model, CAS-ESM2.0 (Chinese Academy of Sciences (CAS), Beijing, China), is at an advanced global level [8]. Three fundamental elements constitute the basic models of Earth system simulation: System Dynamics (SD) models, Cellular Automata (CA) models, and Agent-Based (AB) models. Each has its own characteristics and complementary nature, allowing for organic integration into the basic model of Earth system simulations, with CA being an essential component [9]. The spherical grid model used in this study is a type of CA model.

The Earth Tessellation Grid (ETG) belongs to the traditional research field of Earth system science. An ETG is a spherical (ellipsoidal) grid that can be subdivided infinitely without changing its shape, providing a fitting mesh for the Earth [10]. Recently, the study of grids for digital earth platforms has emerged as a new research field. It emphasizes the establishment of a unified and rigorous global positioning reference system, the fusion and integration of multi-source and heterogeneous spatial data and related thematic data, the construction and analysis of three-dimensional virtual geographic environments, and the simulation and inference of various geographical spatial processes. There are two types of grids used in digital Earth platforms: two-dimensional spherical surface grids (DGGs, Discrete Global Grids) and three-dimensional spherical grids (ESSG). Nearly 20 DGG schemes [11] are used for organizing surface spatial data. This study mainly involves three-dimensional spherical grids. The main achievements in this field include three types: Spheroid Degenerated Octree Grid (SDOG) [12], Sphere Geodesic Octree Grid (SGOG) [13,14], and Sphere Shell Space Grid (S3G) [15], all proposed by Chinese scholars. SDOG and S3G belong to the Latitude–Longitude Hexahedral Grids, while

SGOG belongs to the Geodesic Tetrahedron Grid, which have certain advantages in a true three-dimensional modeling of geographic space, especially in the true three-dimensional modeling of the Earth's crust, and SGOG grids can be directly extended to ellipsoids. Therefore, in this study, the SGOG grid was selected as the basic model for watershed crustal modeling. It should be noted that the computational grids (vectors) of Earth system models and the grids (rasters) of digital Earth platforms do not fundamentally differ. The organic integration of the two can be achieved [16–18]. In recent years, despite strong interest in research and commercial applications of Discrete Global Grid Systems (DGGS), participation from the GIS scientific community has remained focused on relatively narrow topics, such as grid specifications and refinement improvements [19]. Recent advancements include: theoretical developments in multi-resolution encoding for hexagonal discrete grids [20,21]; the optimization and extension of grid subdivision and encoding methods [22–27]; the analysis of grid metrics and their applications [28,29]; reviews and challenges in DGGS research [19,30]; spatial analysis [31,32]; coastal environment and maritime applications [33,34]; terrain analysis [35,36]. See Table 1.

**Table 1.** Characteristics of different types of grids.

Grid Type	Representative References	Advantages	Disadvantages	Application
Triangle	Alborzi and Semmet, 2000 [37]; Bartholdi, 2001 [38]; Baumgarder, 1985 [39]; Dutton, 1984 [40], 1999 [41]; Fekete and Treinish, 1990 [42]; Goodchild and Yang, 1992 [43]; Song, 2002 [44]; White, 1998 [45]	Can be combined into arbitrary polygons; completely cover spherical surfaces; easy for texture mapping; effectively fits curved surfaces; addresses convergence issues at poles; preservation of similarity, edge length, and area equality.	Non-uniformly adjacent units; not unique directions; do not align with traditional square conventions and output devices.	Modeling and visualization of large-scale geographic spatial data
Quadrilateral	Sahr, 2003 [46]; White 2000 [47]; Björke, 2003 [48]; Gibb, 2016 [49]	Simpler geometric structures; consistent directional, radial symmetry, and translational congruence properties; can directly leverage many algorithms based on plane quadtrees; well-matched with traditional output devices.	Non-uniform adjacency; inability to cover the entire globe; inability to directly generate spherical grids; significant distortion or degeneration of units in high-latitude regions.	Storage and management of spatiotemporal big data
Hexagon	Heikes, 1995 [50]; Sadourny, 1968 [51]; Sahr, 2003 [46]; Thuburn, 1997 [52]; Peterson, 2006 [53]; Vince, 2006 [54]; Jin Ben, 2018 [20]	The most regular structure, highest plane coverage and angular resolution; consistent topology; topological distance closely matches Euclidean linear distance; highest spatial sampling rate;	Cannot fully cover the spherical surface; faces challenges in encoding efficiency of grid cells and compatibility with constructing multi-resolution data models.	Certain advantages in dynamic modeling and Earth system model computations

The Earth's surface serves as the interface between the atmosphere and lithosphere, and is the focal area for various geographical phenomena and processes. Geomorphology is pivotal to Earth's surface science and tightly integrates disciplines such as human dynamics, biology, biogeochemistry, geochemistry, geology, hydrology, geomorphology, and atmospheric dynamics [55]. Information regarding the topography of the Earth is a critical parameter for nearly all Earth science analyses, precise land use, and planning [56]. Understanding surface processes relies on modern digital terrain representation [57], and contemporary ground, aerial, and space remote sensing technologies have enabled the detailed geographic analyses of large regions, or even globally [58].

In the field of global discrete grids, there exists a predominance of theoretical research over applied studies. Issues in digital watershed three-dimensional spatial modeling and geographical process simulation include traditional watershed 2.5D spatial modeling, which prioritizes surface over subsurface, focusing mostly on surface geographical pro-

cesses, thereby posing challenges in simulating and analyzing sub-surface spatial processes and phenomena within watersheds. Moreover, existing three-dimensional simulation platforms are segmented and disconnected, failing to integrate surface, near-surface, and subsurface spaces into unified modeling. Traditional geographical simulation methods often operate at fixed scales, aiming primarily for single-scale simulations, with intricate complexities in scale integration and variation. From the perspective of river simulators, macro-level framework studies predominate, with limited attention to specific technical mechanisms. Spherical grid partitioning effectively addresses scale issues. Its recursive subdivision mechanism facilitates the construction of models at single scales and hybrid multi-level scales, thus enabling the flexible and on-demand simulation of watershed geographical processes.

In summary, this study focuses on the construction of a true three-dimensional computational platform for the Yellow River Simulator based on SGOG grids, globally shared Digital Elevation Model (DEM) data and watershed terrain and landform data. It tackles key technical challenges in building a spherical grid multi-scale model and dynamic simulation computing technology for watershed geographical processes. The study verifies these technologies through experiments, particularly in simulating groundwater point source pollution diffusion, aiming to provide essential technical support and foundations for constructing the Yellow River Simulator.

## 2. Technical Foundations of True 3D Yellow River Simulation Platform Construction

### 2.1. SGOG Subdivision Theory

The Earth Tessellation Grid fundamentally treats the Earth system as a regular geometric fluid, recursively dividing the flow surface or fluid into quasi-uniform segments, organically encoding (indexing) and organizing them to simulate Earth phenomena and processes. Each grid consists of grid points, edges, centers, and elements (surface and volume elements). The SGOG adopts a method of large circular arc median QTM octree division (spherical quadtree and radial binary tree), where the spherical quadtree can utilize any existing QTM encoding scheme (this study uses directional encoding), and the radial aspect employs binary tree encoding (Figure 1). The SGOG grid (tile) system was relatively evenly distributed, and symmetric with respect to the center of the sphere, exhibiting simple regularity and consistent topological relationships. The intralayer deformation is minimal, whereas the radial deformation is significant [13,14]. Matching the grid points of the Earth's surface with the basin's DEM elevation through interpolation (this study employs the nearest neighbor method), and subsequently connecting the grid edges, can express the basin's landform. Introducing basin geological strata data (assumed data in this study) and matching them with the underground grid can convey information related to the basin's underground geological strata, thereby establishing a truly three-dimensional crustal simulation platform for the Yellow River Basin.

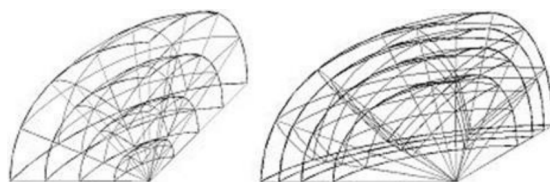


**Figure 1.** Spherical Quadtree (QTM) Grid.

### 2.2. Study Area and Source Data

The Yellow River originates from the northern foot of the Bayan Har Mountains on the Qinghai–Tibet Plateau, has a total length of approximately 5464 km, and flows through more than 370 counties in nine provinces before emptying into the Bohai Sea. The basin covers an area of 795,000 square kilometers, making it the fifth-longest river in the world and the second-longest river in China. It is considered one of the most difficult rivers to manage globally. The Yellow River Basin traverses three major terraces spanning vast distances,

with numerous mountain ranges and significant east–west elevation differences, leading to marked variations in landforms. Sediment deposition poses a prominent challenge, exacerbating the sharp conflict between human activities and water resources within fragile ecological environments. Historically, the Yellow River has served as the cradle of Chinese civilization, representing a hub for political, economic, and cultural activities. However, the overall socioeconomic development of the region lags behind the national average in today’s comprehensive societal and economic context.

Considering the computational and storage capabilities of a single machine, the modeling is based on the SGOG 9th, 10th, 11th, and 12th level subdivision tiles (corresponding to approximate grid surface edge lengths of 19.49 km, 9.75 km, 4.87 km, and 2.44 km, respectively). DEM data covering the Yellow River basin area were downloaded from the shared website (<http://www.ncdc.ac.cn/>, accessed on 1 March 2023), specifically the SRTM v4.1 data with a 30 m resolution. The basic parameters included the UTM/WGS-84 projection, GeoTIFF format,  $84,467 \times 34,894$  pixels, with elevations relative to the geoid of the WGS-84 ellipsoid.

### 2.3. Technical Approach for Simulation Platform Construction

This study adopts Visual Studio 2017 (VS2017) as the development platform, utilizes the open-source 3D graphics toolkit Open Scene Graph(OSG) as the graphics engine, employs standard C++ as the development language, and utilizes the Interactive Data Language (IDL) to process the DEM source data to establish the experimental environment. Initially, we conducted computations and conversions of the SGOG tile grid point coordinates, matched the longitude and latitude coordinates with the DEM grid, and then proceeded with grid point elevation interpolation calculations and stratigraphic data matching. Subsequently, hybrid multiscale grid modeling was performed, followed by hierarchical color rendering. The overall technical approach is illustrated in Figure 2.

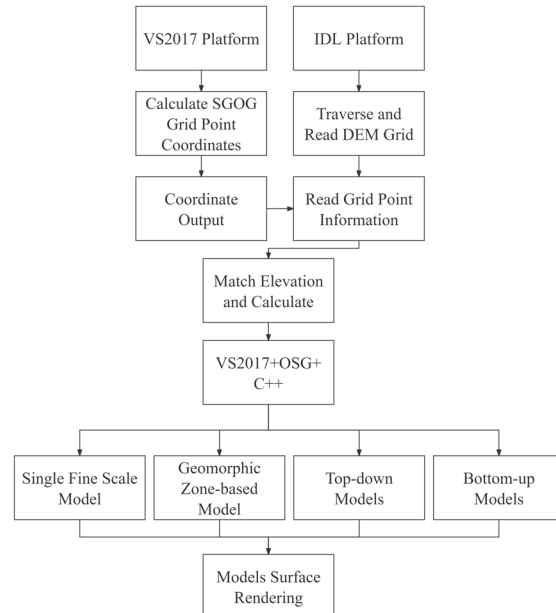


**Figure 2.** Overall technical approach for constructing the adaptive multiscale three-dimensional crustal simulation platform for the Yellow River.

### 3. Construction Process of Adaptive Multiscale True 3D Simulation Platform

The characteristics of the large-volume, multidimensional spatiotemporal nature, heterogeneous multi-source, and dynamic variability of Earth’s spatiotemporal big data, as well as the complexity and comprehensiveness of Earth system simulation, demand that the Earth system simulation platform be targeted, adaptive, and flexible, enabling agile spatiotemporal multiscale, multidimensional simulations for specific simulation

requirements. This section introduces the construction process and the results of the construction of an adaptive multiscale true three-dimensional simulation platform for spherical grids. The experimental environment for this study includes: 12th Gen Intel Core i5-12450H 2.00 GHz processor, 3200 MHz 32 GB RAM, NVIDIA GeForce RTX 3050 graphics processor, 512 GB PCIe solid state drive; Windows 11 operating system, Visual Studio 2017 Professional, OSG 3.4.1 open source library, QT 5.12.0 open source library, QT Visual Studio Tools v2.10.1.2 extension tools; and is developed using C++ as the programming language.

### 3.1. Establishment of Single Fine-Scale Grid Simulation Platform

DEM and ETG are essentially based on the discrete representation of geographic space through sampled points. Naturally, a higher sampling density leads to a higher expression accuracy. Owing to the limitations of the computational power available in this study, the maximum level of SGOG grid partitioning allowed the entire Yellow River Basin crustal simulation to be at the 12th level. To provide a comparative benchmark for the various modeling methods, the results of the Yellow River simulation platform were obtained following the aforementioned technical approach, as shown in Figure 3. Using the mean elevation of each surface triangular grid point as an index, the corresponding thresholds were set and hierarchical color rendering was performed based on different threshold levels, resulting in the rendering of the Yellow River Basin, as shown in Figure 4. A side view of the rendering is displayed in Figure 5, where the curvature of the Yellow River Basin's crust and the vertical stratigraphic structure can be observed. A local zoomed-in view is shown in Figure 6.



**Figure 3.** Modeling results of the 12th layer single-scale grid in the Yellow River Basin.

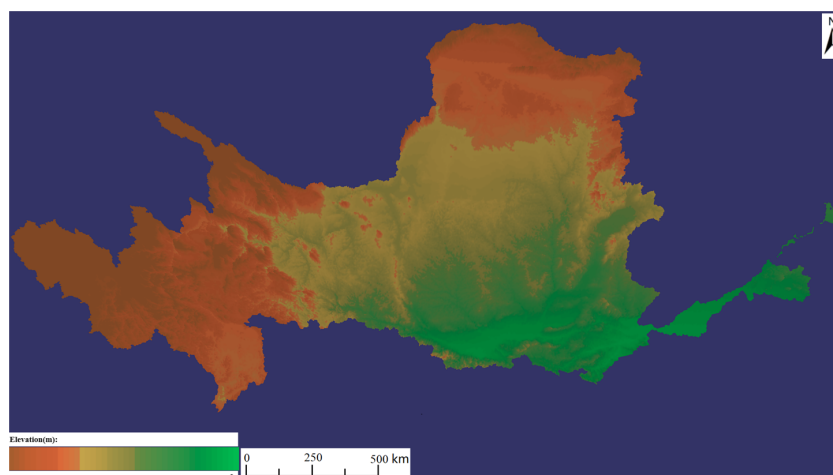


**Figure 4.** Rendering of the 12th layer single-scale grid model in the Yellow River Basin.

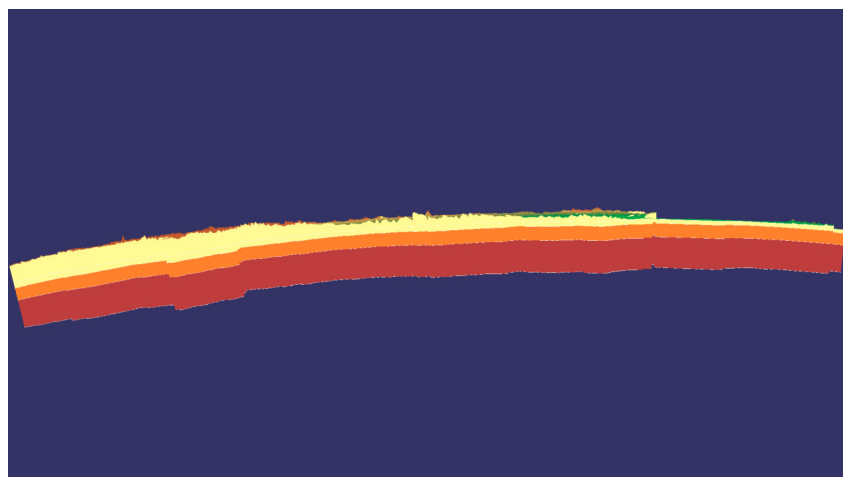


**Figure 5.** Side view of the rendering effect of the 12th layer single-scale model in the Yellow River Basin (stratigraphic data are hypothetical).

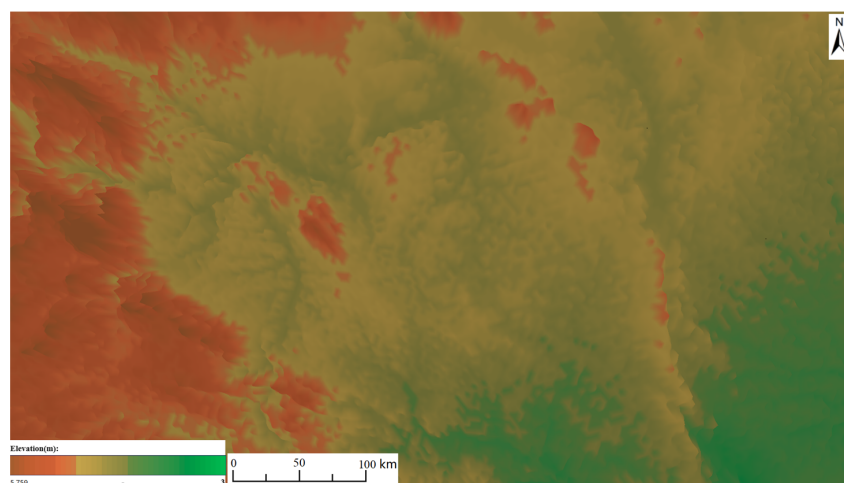


**Figure 6.** Local magnification of the rendering effect of the 12th layer single-scale model in the Yellow River Basin.

### 3.2. Establishment of Adaptive Multiscale Simulation Platform Based on Geomorphic Zoning

The Yellow River Basin has a fixed geomorphic pattern and structure. The boundaries of the geomorphic divisions in the Yellow River Basin were downloaded from the National Cryosphere Desert Data Center (<http://www.ncdc.ac.cn/>, accessed on 1 March 2023) and overlaid with the DEM. The geomorphic divisions were then clipped according to the DEM. Based on different geomorphic types, the corresponding grid layers were manually designated and adjacent layers were merged to create an adaptive multiscale Yellow River simulation platform based on divisions, as shown in Figure 7. On this platform, the Qinghai–Tibet Plateau, Qinling Mountains, and downstream areas were divided into 12 layers, whereas the Loess Plateau, Yinshan Mountains, Liupan Mountains, Lvliang Mountains, and Taihang Mountains were divided into 11 layers. The Ordos Plateau, Hetao Plain, Guanzhong Basin, Fen River Valley, and Taiyuan Basin were divided into 10 layers, and the downstream North China Plain was divided into the 9th layer. It should be noted that because of the narrow channel area in the downstream region, even with the use of a 12-layer grid for matching, there are still a few places where matching is unsuccessful, resulting in discontinuities.

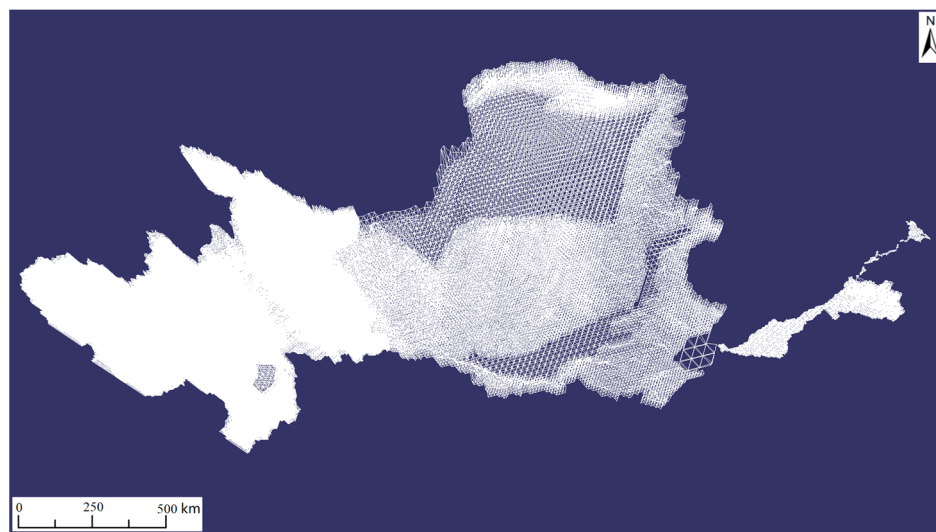


**Figure 7.** Hybrid multiscale grid modeling results in the Yellow River Basin, based on geomorphic zoning.

The technical approach for grid model edge matching in different geomorphic regions is as follows: The boundary portions of the grid model of each division were extended outward by a certain distance and overlaid. Duplicate grids were identified and removed.

### 3.3. Establishment of Top-Down Adaptive Multiscale Simulation Platform

A top-down modeling approach was implemented, starting from coarser grids and automatically subdividing them into finer grids according to specific rules until the desired level of detail is achieved. In this method, the 9th to 12th layers of the SGOG grid were selected to model the entire basin.

(1) Initially, an appropriate subdivision level  $n$  was selected to model the entire Yellow River Basin. This subdivision level was determined based on the specific scale of the study area, with  $n = 9$  (approximating a triangle edge length of 19.49 km) chosen for the initial modeling of the entire basin.

(2) After elevation matching, a threshold value  $\Delta$  for the maximum height difference between grid points is set as the criterion for further subdivision. The threshold  $\Delta$  is determined based on the overall topography of the current basin. In this study, threshold values of 50 m, 100 m, and 150 m were used for  $\Delta$ . If the height difference exceeded this threshold, the grid was further subdivided; otherwise, the subdivision was halted. The specific method for subdivision involved connecting the midpoints of the three edges of triangles at the current level to create four new triangles at level  $n + 1$ .

(3) The elevation differences between pairs of vertices on the outer grid are calculated, and the values are compared against the threshold  $\Delta$  to determine whether to retain or subdivide. A technical roadmap for this method is shown in Figure 8.

To facilitate model comparison, this study employed two methods: the fixed and variable threshold step methods.

(a) Fixed threshold step method: This method consists of three variations ranging from the 9th layer to the 12th layer. The elevation difference threshold between adjacent layers was set at 50 m, 100 m, and 150 m to model the Yellow River simulation platform.

(b) Variable threshold step method: This method includes two variations. The first variation starts with a 50 m threshold at the 9th–10th layers and increases by 50 m at each step, until reaching a 150 m threshold at the 11th–12th layers. The second variation begins with a 150 m threshold at the 9th–10th layers and decreases by 50 m at each step, until reaching a 50 m threshold at the 11th–12th layers.

The results of the aforementioned experiments are illustrated in Figure 9.



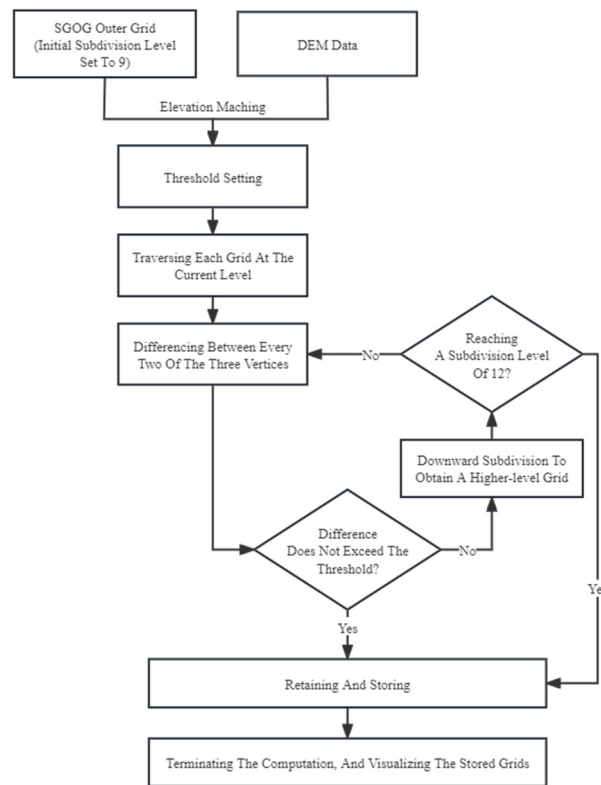


**Figure 8.** Technical roadmap for the top-down approach.

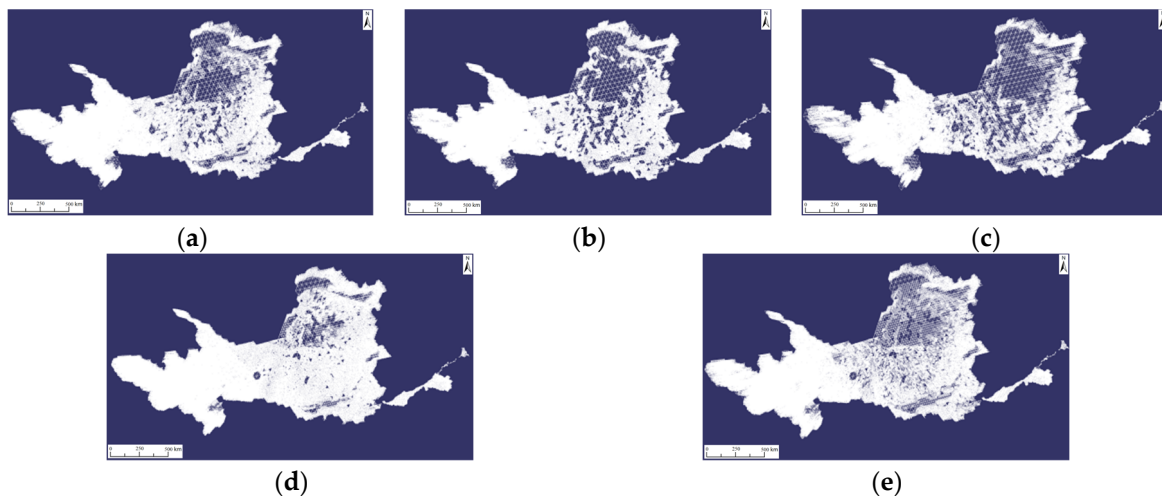


**Figure 9.** Crustal grid modeling results in the Yellow River Basin under different elevation difference thresholds in the top-down approach. (a). Fixed threshold at 50 m. (b). Fixed threshold at 100 m. (c). Fixed threshold at 150 m. (d). Variable threshold range: 50 m–100 m–150 m. (e). Variable threshold range: 150 m–100 m–50 m.

In the top-down approach, the magnitude of the threshold determines grid density. A larger threshold resulted in sparser grids, whereas a smaller threshold resulted in denser grids. Furthermore, the different geomorphic types exhibited varying grid density patterns. In practical applications, the choice of threshold values can be based on specific requirements.

The partial subdivision code statements for the top-down algorithm are as follows:

// The three points with height differences greater than the threshold, as well as their three child points, will be divided.

```

if (abs(H1 - H2) >= HD || abs(H2 - H3) >= HD || abs(H3 - H1) >= HD) {
  B4 = (B1 + B2)/2;
  B5 = (B2 + B3)/2;
  B6 = (B3 + B1)/2;
  L4 = (L1 + L2)/2;
  L5 = (L2 + L3)/2;
  L6 = (L3 + L1)/2;
}

```

The latitude and longitude coordinates of the grid points with height differences exceeding the threshold are subdivided in the manner described above.

### 3.4. Establishment of Bottom-Up Adaptive Multiscale Simulation Platform

The bottom-up modeling approach, which progresses from finer to coarser grids, shares the basic principles of the top-down method, but in the opposite direction, merging from higher to lower subdivision levels. Initially, the finest grid model (designated the 12th layer in this study) was established. Starting from the bottom, the maximum height difference between the grid points on the outer layers was evaluated at each level to determine whether it was below a predefined threshold. If this occurred, the grids were merged until an appropriate level was reached. In this method, grids at subdivision levels 9, 10, 11, and 12 were selected to model the entire basin. Threshold values of 50 m, 100 m, and 150 m were used in separate experiments along with the variable threshold experiments. The technical roadmap of this method is shown in Figure 10, and the modeling results are presented in Figure 11.

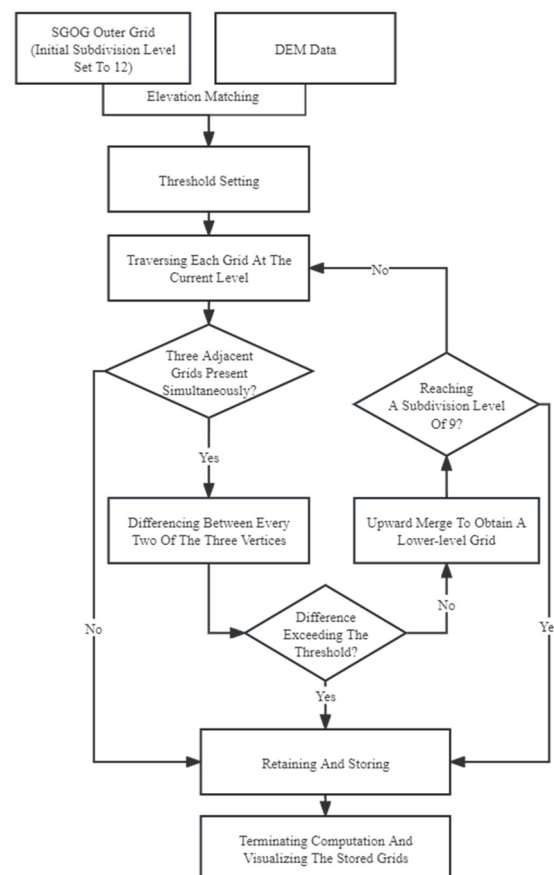
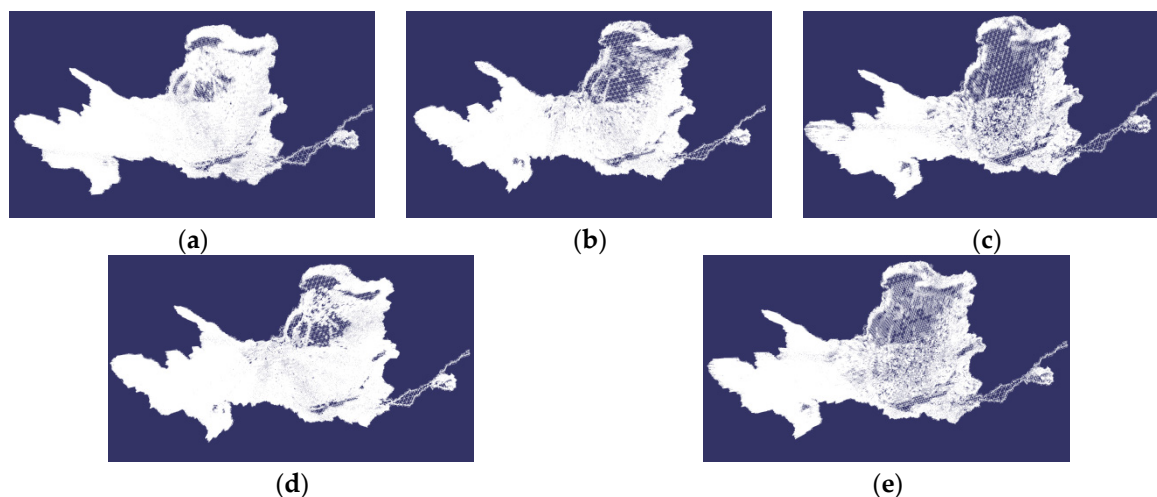


Figure 10. Technical roadmap for the bottom-up approach.



**Figure 11.** Crustal grid modeling results in the Yellow River Basin under different elevation difference thresholds in the bottom-up approach. (a). Fixed threshold at 50 m. (b). Fixed threshold at 100 m. (c). Fixed threshold at 150 m. (d). Variable threshold range: 50 m–100 m–150 m. (e). Variable threshold range: 150 m–100 m–50 m.

Compared to Figure 9, the bottom-up approach for crustal modeling in the Yellow River Basin generally produces denser grids, providing a more comprehensive representation of terrain details. The algorithm and code implementation of this method approximate the top-down approach, and will not be reiterated here.

#### 4. Comprehensive Evaluation of Hybrid Multiscale Grid Models in the Yellow River Basin

The above experiments employed four methods, namely single-scale, geomorphic zoning, top-down, and bottom-up, to flexibly construct the 12th layer of the finer SGOG crustal grid model and the 11 other adaptive hybrid multiscale SGOG grid models in the Yellow River Basin. These models exhibit diverse appearances. To objectively evaluate the merits and demerits of each method, this study conducted a quantitative evaluation from two perspectives, terrain information representation and algorithmic consumption, providing scientific references for the construction of a geographic simulation platform for the basin.

##### 4.1. Selection of Evaluation Indicators

In general, the greater the amount of terrain information implied by the surface model, the more realistic and higher quality the effect. Based on the characteristics of the DEM data and the principle of easy calculation, this study selected three indicators, namely, terrain roughness, elevation variation coefficient, and terrain relief, to measure the amount of terrain information contained in the model. For comparison, this study also lists the standard deviation and mean elevation. In addition, to establish a watershed simulation platform, the efficiency of model construction is also an important indicator of its quality from a practical perspective. This study selected four modeling efficiency indicators: grid vertex count, modeling time consumption (calculated uniformly after the grid vertex elevation is matched), grid point coordinate file storage space consumption (hereafter referred to as file storage space consumption), and running memory space consumption. Using the 12th layer grid model as a reference, a quality index calculation, comparison, and ranking of the remaining 11 hybrid scale models were conducted, thus comprehensively evaluating the terrain information expression and model operating efficiency of the aforementioned hybrid multiscale models.

The grid vertex count is the total number of vertices on the outermost surface grid for single-layer or hybrid multiscale modeling. The terrain roughness formula used in this study is as follows:

$$\sigma = \frac{A}{A_p} \quad (1)$$

where  $A$  is the sum of the surface area on the watershed grid and  $A_p$  is the sum of the lower surface area of the watershed grid, representing the projected area of the watershed surface grid on the sphere.

Mean elevation: The mean elevation is the sum of the elevations of all grid vertices divided by the number of grid vertices, and reflects the average level of elevation in the region.

$$\bar{H} = \frac{\sum_{i=1}^n H_i}{n} \quad (2)$$

where  $H$  is the elevation of the grid vertex, and  $n$  is the number of grid vertices.

Elevation standard deviation:

$$s = \sqrt{\frac{\sum (H - \bar{H})^2}{n - 1}} \quad (3)$$

Elevation variation coefficient: the percentage of the ratio of elevation standard deviation to mean elevation, reflecting the degree of deviation of a set of elevation values from the mean.

$$c \cdot v = \frac{s}{\bar{H}} \times 100\% \quad (4)$$

Terrain relief:

$$R = H_{max} - H_{min} \quad (5)$$

In this formula,  $H_{max}$  is the highest elevation value in region, and  $H_{min}$  is the lowest elevation value in region.

Time consumption refers to the time elapsed from the start of the program to the completion of the generation process after completing grid elevation matching, including processes such as grid data reading, grid data calculation, scene rendering, and generation. File storage space consumption and running memory space consumption refer to the computer hard disk space consumed by storing grid data in file form for different methods and the computer running memory consumed by calculating, drawing, and visualizing grid data in the program for different methods.

#### 4.2. Definition of Quality Indices

The crustal model of the Yellow River Basin constructed in the previous section is most finely represented by the 12th layer grid model. Based on this, the quality standard for the hybrid multiscale model is defined as follows: the model with the closest amount of terrain information to the 12th layer grid model and the highest modeling and computing efficiency is of the best quality.

Definition of the quality index: Let the aforementioned indicators be denoted as  $m_i$  and the corresponding indicator for the 12th layer as  $m_{n=12}$ . The quality index  $w_i$  is defined as the absolute difference between  $m_i$  and  $m_{n=12}$  divided by  $m_{n=12}$ , that is:

$$w_i = \frac{|m_i - m_{n=12}|}{m_{n=12}} \times 100\% \quad (6)$$

Each indicator has a different influence on the quality of the model relative to the aforementioned quality standards and indicators. The quality index for terrain information-related indicators is better when is smaller, whereas a larger quality index is preferable for efficiency-related indicators. These are referred to as negative and positive indicators,

respectively. Accordingly, the negative and positive quality indices,  $Q_1$  and  $Q_2$ , are defined as follows:

$$Q_1 = \sum w, w \in \{w_{TerrainRoughness}, w_{TerrainRelief}, w_{ElevationVariabilityCoefficient}\} \quad (7)$$

$$Q_2 = \sum w, w \in \{w_{NumberOfGridVertices}, w_{TimeConsumption}, w_{FileStorageSpace}, w_{RuntimeMemorySpace}\} \quad (8)$$

The quality of each hybrid model was comprehensively determined based on the ranking of  $Q_1$  and  $Q_2$ .

### 4.3. Computational Results and Evaluation Analysis

For convenience of analysis and comparison, the experimental numbers for the aforementioned experiments are as follows (Table 2):

**Table 2.** Model construction experiment labeling.

Labeling	A	B	C	D	E	F
Experiment	Single-scale 12th Layer	Terrain-based Partitioning Method	Top-down Threshold 50 m	Top-down Threshold 100 m	Top-down Threshold 150 m	Top-down Threshold 50–100–150 m
Labeling	G	H	I	J	K	L
Experiment	Top-down Threshold 150–100–50 m	Bottom-up Threshold 50 m	Bottom-up Threshold 100 m	Bottom-up Threshold 150 m	Bottom-up Threshold 50–100–150 m	Bottom-up Threshold 150–100–50 m

#### 4.3.1. Terrain Feature Representation

The calculations of the terrain information-related indicators for various scale models of the Yellow River Basin crust are presented in Table 3. Overall, it can be seen that the terrain information-related parameters for various hybrid scale models are not significantly different from the single 12-layer scale model (Method A). The terrain roughness was slightly lower than that of Model A, indicating that regardless of the hybrid scale used, a certain amount of terrain relief details were omitted. The elevation variation coefficient for Model B based on geomorphic zoning was greater than that of Model A, whereas the rest were lower than that of Model A. This indicates that, in terms of standard deviation and mean elevation, Model B has a larger standard deviation and a smaller mean elevation. The other methods had larger elevation standard deviations and mean elevations, indicating that the continuity of the elevation distribution in Model B was not as good as that in the other models. The terrain relief for the bottom-up approach was equivalent to that of Model A, whereas those of the other methods were slightly lower. In particular, the top-down and bottom-up methods have fixed values, reflecting a certain determinism in the modeling mechanism of each method. Figure 12 is shown below.

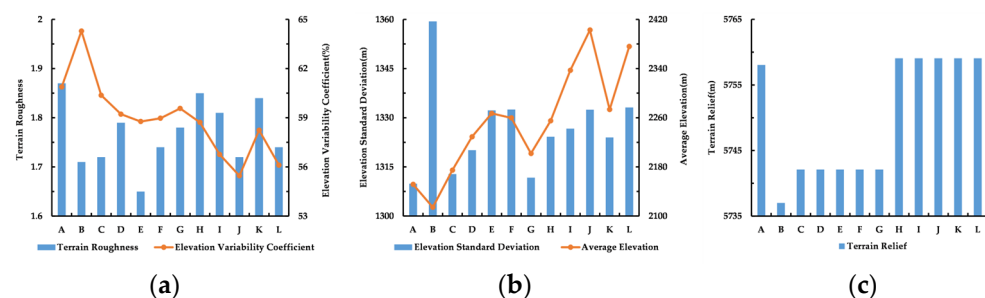


**Figure 12.** Terrain feature representation. (a): Terrain roughness and elevation variability coefficient. (b): Elevation standard deviation and average elevation. (c): Terrain relief.

**Table 3.** Terrain information-related (negative) indicators.

Methods	Labeling	Terrain Roughness	Elevation Standard Deviation (m)	Average Elevation (m)	Elevation Variability Coefficient (%)	Terrain Relief (m)
Single-scale	A	1.87	1309.86	2151.55	60.88	5758.05
Geomorphic Zoning	B	1.71	1359.38	2114.33	64.29	5737.01
Top-down (from coarse to fine)	C	1.72	1312.81	2174.71	60.37	5742.11
	D	1.79	1320.10	2228.97	59.22	5742.11
	E	1.65	1332.22	2267.01	58.77	5742.11
	F	1.74	1332.50	2259.69	58.97	5742.11
	G	1.78	1311.71	2201.86	59.57	5742.11
Bottom-up (from fine to coarse)	H	1.85	1324.20	2255.05	58.72	5759.07
	I	1.81	1326.67	2337.15	56.76	5759.07
	J	1.72	1332.44	2402.66	55.46	5759.07
	K	1.84	1323.98	2273.36	58.24	5759.07
	L	1.74	1333.11	2376.00	56.11	5759.07

#### 4.3.2. Computational Efficiency

The calculations of the model operating efficiency-related indicators for the various scale models of the Yellow River Basin crust are listed in Table 4. It can be observed that the temporal and spatial consumption of the model computation is directly related to the number of grid vertices; the greater the number of vertices, the higher the temporal and spatial consumption. Among them, Model B had the fewest grid vertices, resulting in the lowest temporal and spatial consumption and the highest efficiency. It is important to emphasize that the watershed simulation platform consists of a series of logical steps, as shown in Figure 1. Time consumption refers to the visualization construction time of the grid model after the elevation matching of all grid points, excluding the time consumed for processing the source DEM data, calculating grid point coordinates, matching grid point elevations, overlaying geomorphic boundaries with the source DEM, data clipping, and the hierarchical color rendering of the model. For example, in the experimental environment of this study, single-scale Model A required approximately 3.5 h from grid point coordinate calculation, elevation matching, and grid generation to color rendering. Figure 13 is shown below.

**Table 4.** Model operating efficiency-related (positive) indicators.

Methods	Labeling	Number of Grid Vertices	Time Consumption (s)	File Storage Space Consumption (MB)	Runtime Memory Space Consumption (MB)
Single-scale	A	91,327	2.95	50.5	1024.0
Geomorphic Zoning	B	51,692	1.73	28.1	626.1
Top-down (from coarse to fine)	C	79,930	2.72	45.3	1009.3
	D	67,521	2.47	41.2	917.9
	E	53,581	2.21	36.8	819.9
	F	65,068	2.46	41.0	913.5
	G	63,496	2.45	40.8	909.0
Bottom-up (from fine to coarse)	H	86,021	2.93	48.9	1016.0
	I	73,544	2.56	42.7	951.4
	J	61,917	2.39	39.9	889.0
	K	85,451	2.87	47.9	1015.2
	L	63,453	2.43	40.5	902.3

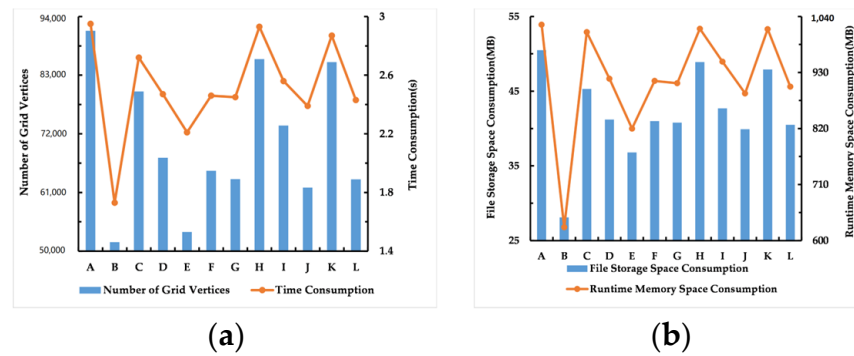


**Figure 13.** Computational efficiency. (a): Number of grid vertices and time consumption. (b): File storage space consumption and runtime memory space consumption.

### 4.3.3. Quality Indices

The quality index calculations for these indicators are presented in Tables 5 and 6.

**Table 5.** Quality index for terrain information-related indicators.

Methods	Labeling	$W_{\text{TerrainRoughness}}$ (%)	$W_{\text{ElevationVariabilityCoefficient}}$ (%)	$W_{\text{TerrainRelief}}$ (%)	$Q_1$ (%)	Ranking
Geomorphic Zoning	B	8.56	5.60	0.37	14.53	8
Top-down (from coarse to fine)	C	8.02	0.84	0.28	9.14	5
	D	4.28	2.73	0.28	7.29	4
	E	11.76	3.47	0.28	15.51	10
	F	6.95	3.14	0.28	10.37	7
	G	4.81	2.15	0.28	7.24	3
Bottom-up (from fine to coarse)	H	1.07	3.55	0.02	4.64	1
	I	3.21	6.77	0.02	10.00	6
	J	8.02	8.90	0.02	16.94	11
	K	1.60	4.34	0.02	5.96	2
	L	6.95	7.84	0.02	14.81	9

**Table 6.** Quality index for model operating efficiency indicators.

Methods	Labeling	$W_{\text{NumberOfGridVertices}}$ (%)	$W_{\text{TimeConsumption}}$ (%)	$W_{\text{FileStorageSpace}}$ (%)	$W_{\text{RuntimeMemorySpace}}$ (%)	$Q_2$ (%)	Ranking
Geomorphic Zoning	B	43.40	41.36	44.36	38.86	167.98	1
Top-down (from coarse to fine)	C	12.48	7.80	10.30	1.43	32.01	9
	D	26.07	16.27	18.42	10.36	71.12	7
	E	41.33	25.08	27.13	19.93	113.47	2
	F	28.75	16.61	18.81	10.79	74.96	6
	G	30.47	16.95	19.21	11.23	77.86	5
Bottom-up (from fine to coarse)	H	5.81	0.68	3.17	0.78	10.44	11
	I	19.47	13.22	15.45	7.09	55.23	8
	J	32.20	18.98	20.99	13.18	85.35	3
	K	6.43	2.71	5.15	0.86	15.15	10
	L	30.52	17.63	19.80	11.88	79.83	4

From Table 5, it can be observed that from the perspective of terrain information expression, the bottom-up method is superior to the top-down method, with the geomorphic zoning method ranking in the middle and later positions. Specifically, the bottom-up 50 m threshold (H) and the 50–100–150 m dynamic threshold (K) models rank in the top two positions, while the top-down 150–100–50 m dynamic threshold (G) and the 100 m fixed threshold (D) models rank 3rd and 4th, and the scores of the two are basically comparable. The top-down 50 m fixed threshold (C), bottom-up 100 m fixed threshold (I), and top-down

50–100–150 m dynamic threshold (F) models had similar scores, ranking 5th to 7th, and the geomorphic zoning method (B) ranks 8th. Finally, the bottom-up 150–100–50 m dynamic threshold (L), top-down 150m fixed threshold (E), and bottom-up 100m fixed threshold (J) models rank 9th to 11th. The quality indices for rankings 8–11 were all greater than 14 and were essentially in the same category. Figure 14 is shown below.

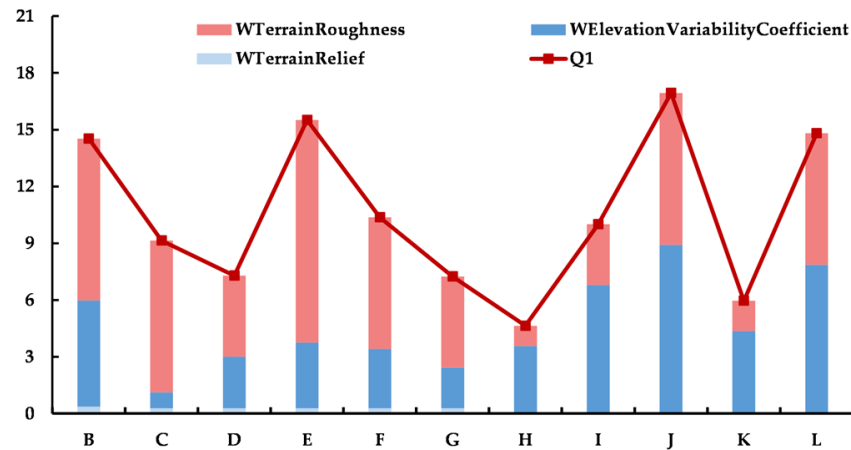


Figure 14. Quality index for terrain information-related indicators.

As shown in Table 6, from the perspective of computational efficiency, the quality ranking is almost the opposite of that in Table 4. The geomorphic zoning method performed the best, and the top-down approach was superior to the bottom-up approach. Specifically, Model B demonstrated an outstanding performance, with the highest score. Model E was on par with Model B, with scores over 100. Models J, L, G, F, and D belonged to the second tier, with scores ranging from 70 to 90. Models I and C fell in the third tier, with scores ranging between 30 and 60. Models K and H were in the lowest tier, with scores below 20. Figure 15 is shown below.

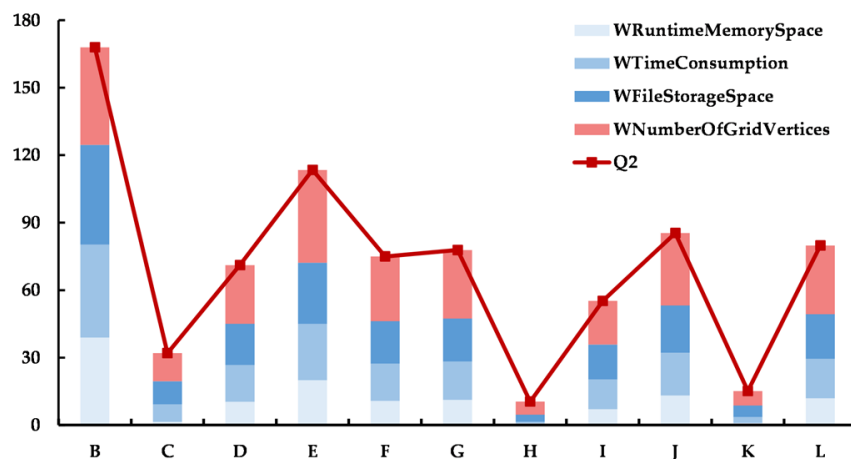


Figure 15. Quality index for model operating efficiency indicators.

From the above analysis, it can be concluded that, under the given conditions, it is impossible to simultaneously achieve both efficient terrain information representation and computational efficiency in the models. It is a natural and objective law. Each method has its own characteristics, and the selection or achievement of a relative balance between the actual applications and environmental conditions should be based on these characteristics.



## 5. Conclusions

In response to the demands of digital Earth representation and Earth system model computation in the era of spatiotemporal big data, this study utilized SGOG and globally shared DEM data to design and implement a crustal simulation platform for the Yellow River Basin. The platform includes four categories and 12 adaptive multiscale models based on geomorphic zoning, using both top-down and bottom-up approaches. Relevant terrain and computational efficiency indicators were selected to evaluate the quality of grid models in the simulation platforms. The main conclusions are as follows.

- (1) The establishment of a single-scale fine-grid model can reflect terrain details more accurately, approximate actual surface conditions, and provide rich terrain information. However, it requires large amounts of data and high computational power, making it suitable for the precise simulation of surface processes and super-computing environments.
- (2) Adaptive multiscale modeling based on characteristic thresholds achieves an organic balance between terrain feature representation and computational efficiency while maintaining the natural continuity of the terrain. Under the same elevation difference threshold, the bottom-up (finer-to-coarser) approach has certain advantages in terms of terrain feature representation, whereas the top-down (coarser-to-finer) approach excels in computational efficiency. Both approaches can achieve desirable results. These methods provide a certain level of terrain accuracy with relatively relaxed requirements for computational environments, making them widely applicable.
- (3) Geomorphic zoning-based multiscale modeling incorporates prior knowledge of landforms into the modeling process, resulting in stronger targeting. It achieves maximum terrain fidelity in key areas at minimum spatiotemporal cost and exhibits the highest computational efficiency. However, it needs hard boundaries in prior landform zoning, which disrupts the natural continuity of terrain distribution to some extent. Fine-grained landform zoning is required to achieve highly desirable results, which inevitably reduces computational efficiency. This approach integrates human intelligence and incorporates an “attention” mechanism for key areas and issues. This is a crucial technical means of overcoming the bottlenecks in Earth system modeling and geographic process simulation, satisfying the special requirements of complex geographic computations.

In conclusion, the basin crustal simulation platform is a crucial component of the basin simulator. The spherical discrete grid mechanism provides ample flexibility for establishing and applying the platform. The model can be either an arbitrary single scale or adaptive multiscale. The scale can be manually specified or automatically calculated based on the characteristic thresholds. The thresholds can be fixed or dynamic. The construction strategy can proceed from coarser to finer or finer to coarser. This study introduces the concept of a spherical grid-based Yellow River Basin true three-dimensional multiscale simulator platform, addressing the issue of scale rigidity in traditional geographical simulations. It achieves model construction at both a single scale and multiple hierarchical mixed scales, enabling flexible basin geographic process simulations as needed. The platform can be used to organize spatiotemporal big data in the digital Earth context, as well as for Earth system model computations. It encompasses both the static representation of surface phenomena and dynamic simulation of geographic processes. In summary, the Earth’s discrete grid is the core technology of Earth system simulators and represents an important development direction in contemporary Earth information science.

For future research, our team is currently exploring the application of the simulation platform developed in this study to conduct geographic process simulations in the Yellow River Basin, specifically focusing on simulating groundwater point source pollution diffusion based on the Yellow River simulation platform. Other forms of basin geographic process simulations are equally applicable.

**Author Contributions:** Conceptualization, B.L. and J.W.; data curation, J.W.; funding acquisition, J.W.; methodology, B.L.; resources, B.L.; software, Y.Z. and Y.S.; writing—original draft, B.L.; writing—review and editing, B.L., J.W., Y.Z. and Y.S. All authors have read and agreed to the published version of the manuscript.

**Funding:** This research was funded by Henan Key R&D and Promotion Special Program (Science and Technology Tackling) (232102320264). Supported by the Department of Science and Technology of Henan Province, China. Grant number 232102320264.

**Data Availability Statement:** The data presented in this study are openly available in Construction Technique of Spherical Grid-Based Adaptive Multi-scale True 3D Yellow River Simulation Platform Source Code at <https://doi.org/10.57760/sciencedb.16536>.

**Acknowledgments:** We would like to thank all editors and reviewers for their insightful comments, which helped us improve the quality of this paper.

**Conflicts of Interest:** The authors declare no conflicts of interest.

## References

- Zuo, Q.T.; Qiu, X.; Ma, J.X.; Zhang, Z.Z. Evolution of flood control thought and modern flood control strategy in the Yellow-River Basin. *J. Water Resour. Water Eng.* **2023**, *34*, 1–9.
- Xu, X.Y.; Yang, Z.F. General Discussion on Ecological Environment Water Demand. *China Water Resour.* **2003**, *3*, 20–23+5.
- Zuo, Q.T.; Qin, X.; Ma, J.X. Framework Design and Development Layout of Yellow River Simulator Construction. *Yellow River* **2023**, *45*, 18–23.
- Zhang, W. Correctly understand and fully engage with the “River Strategy”. *Water Resour. Dev. Res.* **2023**, *23*, 1–3.
- Xia, J.; Zhan, C.S.; Zeng, S.D.; Zou, L.; She, D.X.; Zuo, Q.T. Theoretical method and practical exploration of Yangtze River Simulator construction. *J. Hydraul. Eng.* **2022**, *53*, 505–514.
- Zhu, A.X.; Zhu, L.J.; Shi, Y.X.; Qin, C.Z.; Liu, J.Z. Integrated watershed modeling and scenario analysis: A new paradigm for integrated study of physical geography? *Prog. Geogr.* **2019**, *38*, 1111–1122. [[CrossRef](#)]
- Wang, H.J.; Zhu, J.; Pu, Y.F. The earth system simulation. *SCIENTIA SINICA Phys. Mech. Astron.* **2014**, *44*, 1116–1126.
- Lu, C.K. Earth system simulation large scientific device to diagnose the Earth. *Invent. Innov.* **2021**, *3*, 57.
- Zheng, X.Q. On the Geographic System Simulation Basic Model. *Chin. J. Nat.* **2012**, *34*, 143–149.
- Zhao, X.S.; Ben, J.; Sun, W.B.; Tong, X.C. Overview of the Research Progress in the Earth Tessellation Grid. *Acta Geod. Cartogr. Sin.* **2016**, *45*, 1–14.
- Zhang, Y.S.; Ben, J.; Tong, X.C. *Theory, Algorithm and Application of Spherical Discrete Grid of Earth Spatial Information*, 1st ed.; Science Press: Beijing, China, 2007; pp. 15–20.
- Wu, L.X.; Yu, J.Q. Global 3D-Grid based on sphere degenerated octree and its distortion features. *Geogr. Geo-Inf. Sci.* **2009**, *25*, 1–4.
- Wang, J.X.; Lu, F.N.; Chen, J. Comparison of surface and solid discrete global grids. *Sci. Surv. Map* **2012**, *37*, 34–36.
- Wang, J.X.; Zheng, Y.S.; Li, Y.H.; Lu, F.N.; Liu, J.N. Building the Platform of Digital Earth with Sphere Split Bricks. *Acta Geod. Cartogr. Sin.* **2015**, *44*, 694.
- Cao, X.F. Research on Earth Sphere Shell Space Grid Theory and Algorithms. Ph.D. Thesis, Information Engineering University, Zhengzhou, China, 2012.
- Zhao, Z.P. Research on Model-oriented Spherical Rhombus Discrete Grids. Master’s Thesis, Nanjing Normal University, Nanjing, China, 2015.
- Liu, K. A Universal Data Model of Discrete Global Grid System Based on Fiber Bundle Theory. Master’s Thesis, Nanjing Normal University, Nanjing, China, 2019.
- Lin, B.X.; Zhou, L.C.; Xu, D.P.; Zhu, A.X.; Lu, G.N. A discrete global grid system for earth system modeling. *Int. J. Geogr. Inf. Sci.* **2018**, *32*, 711–737. [[CrossRef](#)]
- Hojati, M.; Robertson, C.; Roberts, S.; Chaudhuri, C. GIScience research challenges for realizing discrete global grid systems as a Digital Earth. *Big Earth Data* **2022**, *6*, 358–379. [[CrossRef](#)]
- Ben, J.; Li, Y.L.; Wang, R.; Du, L.Y. Algebraic encoding scheme for aperture 3 hexagonal discrete global grid system. *Sci. Earth Sci.* **2018**, *48*, 340–352. [[CrossRef](#)]
- Zhou, J.B.; Ben, J.; Wang, R.; Zheng, M.Y. Encoding and Operation for the Aperture-4 Hexagonal Discrete Global Grids on Uniform Tiles. *J. Wuhan Univ. Inf. Sci. Ed.* **2023**, *48*, 639–646.
- Benjamin, U.; Faramarz, S. Toward volume preserving spheroid degenerated-octree grid. *Geoinformatica* **2020**, *24*, 505–529.
- Liang, X.Y.; Ben, J.; Wang, R.; Liang, Q.S.; Huang, X.H.; Ding, J.J. Construction of rhombic triacontahedron discrete global grid systems. *Int. J. Digit. Earth* **2022**, *15*, 1760–1783. [[CrossRef](#)]
- Zhao, L.; Li, G.; Yao, X.; Ma, Y.; Cao, Q. An optimized hexagonal quadtree encoding and operation scheme for icosahedral hexagonal discrete global grid systems. *Int. J. Digit. Earth* **2022**, *15*, 975–1000. [[CrossRef](#)]
- Zhou, J.B.; Ding, J.J.; Ben, J.; Chen, Y.H.; Liang, Q.S. Multi-mode 3D extension methods for equal-area discrete global grid systems for geospatial data representation. *J. Geod. Geoinf. Sci.* **2024**, *53*, 173–188.

26. Liang, Q.S.; Chen, Y.H.; Ben, J.; Zhou, J.B.; Ding, J.J.; Dai, J.C. Modelling and Storage Method for Hexagonal Remote Sensing Images in Rhombic Triacotahedron Discrete Global Grid System. *J. Geo-Inf. Sci.* **2023**, *25*, 2361–2373.
27. Zhao, L.; Li, G.Q.; Yao, X.C.; Ma, X. Code Operation Scheme for the Icosahedral Hexagonal Discrete Global Grid System. *J. Geoinf. Sci.* **2023**, *25*, 239–251.
28. Wang, Z.; Zhao, X.; Sun, W.; Luo, F.; Li, Y.; Duan, Y. Correlation Analysis and Reconstruction of the Geometric Evaluation Indicator System of the Discrete Global Grid. *ISPRS Int. J. Geo-Inf.* **2021**, *10*, 115. [[CrossRef](#)]
29. Alexander, K.; Ivan, V.; Holger, V.; Evelyn, U. Area and shape distortions in open-source discrete global grid systems. *Big Earth Data* **2022**, *6*, 256–275.
30. Wu, Y.T.; Wan, G.; Liu, L.; Mu, Y.; Wei, Z.J.; Wang, S. A Review of the Research on Discrete Global Grid Systems in Digital Earth. In Proceedings of the IEEE International Information Technology and Artificial Intelligence (ITAC), Chongqing, China, 19 June 2022.
31. Kazemi, M.; Wecker, L.; Samavati, F. Efficient Calculation of Distance Transform on Discrete Global Grid Systems. *ISPRS Int. J. Geo-Inf.* **2022**, *11*, 322. [[CrossRef](#)]
32. Wang, J.X.; Shi, Y.; Qin, Z.L.; Cao, Z.N. A Three-Dimensional Buffer Analysis Method Based on the 3D Discrete Global Grid System. *ISPRS Int. J. Geo-Inf.* **2021**, *10*, 520. [[CrossRef](#)]
33. Bousquin, J. Discrete Global Grid Systems as scalable geospatial frameworks for characterizing coastal environments. *Environ. Model. Softw.* **2021**, *146*, 105210. [[CrossRef](#)] [[PubMed](#)]
34. Andrew, R.; Zoheir, S.; Mario, B. Geospatial Data Analysis for Global Maritime Risk Assessment Using the Discrete Global Grid System. In Proceedings of the 2021 IEEE International Geoscience and Remote Sensing Symposium, Brussels, Belgium, 16 July 2021.
35. Mingke, L.; Heather, M.; Emmanuel, S. Multi-resolution topographic analysis in hexagonal Discrete Global Grid Systems. *Int. J. Appl. Earth Obs. Geoinf.* **2022**, *113*, 102985.
36. Wang, J.X.; Qin, Z.L.; Zhao, G.C.; Li, B.X.; Gao, C.R. Scale Effect Analysis of Basin Topographic Features Based on Spherical Grid and DEM: Taking the Yangtze River as An Example. *J. Basic Sci. Eng.* **2022**, *30*, 1109–1120.
37. Alborzi, H.; Samaet, H. Augmenting SAND with a spherical data model. In Proceedings of the First International Conference on Discrete Global Grids, Santa Barbara, CA, USA, 28 March 2000.
38. Bartholdi, J.J.; Goldsman, P. Continuous indexing of hierarchical subdivisions of the globe. *Int. J. Geogr. Inf. Sci.* **2001**, *15*, 489–522. [[CrossRef](#)]
39. Baumgardner, J.R.; Frederickson, P.O. Icosahedral discretization of the two- sphere. *SIMA J. Numer. Anal.* **1985**, *22*, 1107–1115. [[CrossRef](#)]
40. Dutton, G. Geodesic Modelling of Planetary Relief. *Cartographica* **1984**, *21*, 188–207. [[CrossRef](#)]
41. Dutton, G. *A Hierarchical Coordinate System for Geoprocessing and Cartography*; Springer: Berlin/Heidelberg, Germany, 1999.
42. Fekete, G. Rendering and Managing Spherical Data with Sphere Quadtrees. In Proceedings of the IEEE Conference on Visualization, San Francisco, CA, USA, 26 October 1990.
43. Goodchild, M.F.; Yang, S. A Hierarchical Spatial Data Structure for Global Geographic Information Systems. *Comput. Vis. Graph. Image Process.* **1992**, *54*, 31–34. [[CrossRef](#)]
44. Song, L.; Kimerling, A.J.; Sahr, K. Developing an equal area global grid by small circle subdivision. In *Discrete Global Grids: A Web Book*; Goodchild, M.F., Kimerling, A.J., Eds.; The National Center for Geographic Information and Analysis: Santa Barbara, CA, USA, 2002.
45. White, D.; Kimerling, A.J.; Sahr, K.; Song, L. Comparing Area and Shape Distortion on Polyhedral-Based Recursive Partitions of the Sphere. *Int. J. Geogr. Inf. Sci.* **1998**, *12*, 805–827. [[CrossRef](#)]
46. Sahr, K.; White, D.; Kimerling, A.J. Geodesic Discrete Global Grid Systems. *Cartogr. Geogr. Inf. Sci.* **2003**, *30*, 121–134. [[CrossRef](#)]
47. White, D. Global Grids from Recursive Diamond Subdivisions of the Surface of an Octahedron or Icosahedron. *Environ. Monit. Assess.* **2000**, *64*, 93–103. [[CrossRef](#)]
48. Bjørke, J.T.; Kindlmann, J.K.; Holt, M. A Global Grid Model Based on “Constant Area” Quadrilaterals. In Proceedings of the 9th Scandinavian Research Conference on Geographical Information Science, Espoo, Finland, 4–6 June 2003; pp. 239–250.
49. Gibb, R.; Raichev, A.; Speth, M. The rHEALPix Discrete Global Grid System. 2016. Available online: <https://datastore.landcareresearch.co.nz/dataset/rhealpix-discrete-global-grid-system> (accessed on 17 July 2018).
50. Heikes, R.; Randall, D.A. Numerical Integration of the Shallow-Water Equations on a Twisted Icosahedral Grid. Part II: A Detailed Description of the Grid and an Analysis of Numerical Accuracy. *Mon. Weather Rev.* **1995**, *123*, 1881–1887.
51. Sadourny, R.; Arakawa, A.; Mintz, Y. Integration of the Nondivergent Barotropic Vorticity Equation with an Icosahedral-Hexagonal Grid for the Sphere. *Mon. Weather Rev.* **1968**, *96*, 392–399. [[CrossRef](#)]
52. Thuburn, J. A PV-Based Shallow-Water Model on a Hexagonal Icosahedral Grid. *Mon. Weather Rev.* **1997**, *125*, 2328–2347. [[CrossRef](#)]
53. Peterson, P. Close-Packed Uniformly Adjacent, Multi-resolution Overlapping Spatial Data Ordering. U.S. Patent US8018458B2, 13 September 2011.
54. Vince, A.; Zheng, X. Arithmetic and Fourier Transform for the PYXIS Multi-Resolution Digital Earth Model. *Int. J. Digit. Earth.* **2009**, *2*, 59–79. [[CrossRef](#)]
55. Murray, A.B.; Lazarus, E.; Ashton, A.; Baas, A.; Coco, G.; Coulthard, T.; Fonstad, M.; Haff, P.; McNamara, D.; Paola, C. Geomorphology, complexity, and the emerging science of the Earth’s surface. *Geomorphology* **2009**, *103*, 496–505. [[CrossRef](#)]

- 
56. Dech, S. The Earth surface. In *Utilization of Space*, 1st ed.; Feuerbacher, B., Stoewer, H., Eds.; Springer: Berlin/Heidelberg, Germany, 2005; Volume 1, pp. 53–90.
  57. Tarolli, P.; Arrowsmith, J.R.; Vivoni, E.R. Understanding earth surface processes from remotely sensed digital terrain models. *Geomorphology* **2009**, *113*, 1–3. [[CrossRef](#)]
  58. Yue, T.X. Progress in earth surface modeling. *J. Remote Sens.* **2011**, *15*, 1105–1124.

**Disclaimer/Publisher’s Note:** The statements, opinions and data contained in all publications are solely those of the individual author(s) and contributor(s) and not of MDPI and/or the editor(s). MDPI and/or the editor(s) disclaim responsibility for any injury to people or property resulting from any ideas, methods, instructions or products referred to in the content.